Unsupervised Machine Learning for Identifying Morphological Phenotypes in Abdominal Aortic Aneurysms Using Fully Automated Volume-Segmented Imaging: A Multicentre Cohort Study

Michal Kawka[1,2], Caroline Caradu[3], Ruth Scicluna[4], Colin Bicknell[5], Matthew Bown[4], Manj Gohel[6], Janet T Powell[5], Anna L Pouncey[1,2,5]

1. School of Health & Medical Sciences, City St George's University of London, London, UK
2. St George's Vascular Institute, St George's Hospital, London, UK
3. Vascular Surgery Department, Bordeaux University Hospital, Bordeaux, France.
4. Department of Cardiovascular Sciences and NIHR Leicester Biomedical Research Centre, University of Leicester, Leicester, UK
5. Department of Surgery and Cancer, Imperial College London, London, UK
6. Department of Vascular Surgery, Cambridge University Hospitals, Cambridge, United Kingdom

Correspondence to:

Anna L Pouncey

Department of Surgery & Cancer,

Imperial College London

Ayrton Rd, South Kensington, London SW7 5NH

London, UK

a. a.pouncey@imperial.ac.uk

Background

Thrombo- and microembolic complications following abdominal aortic aneurysm repair are hypothesised to be associated with wall thrombus burden. Fully automatic volume segmentation

(FAVS) of imaging enables extraction of morphological features from which thrombogenic phenotypes may be identified.

Method

This was a multi-centre retrospective cohort study using FAVS to examine pre-operative imaging for elective AAA repairs (2013-2023). Radiological data were matched with National Vascular Registry thromboembolic outcomes data (cerebral, bowel, renal or limb ischaemia). Principal component analysis was used for dimensionality reduction, followed by unsupervised machine learning with k-nearest neighbours (kNN) clustering, with number of clusters determined using silhouette scores. Clusters were compared using multivariate logistic regression, adjusting for aortic size index, cardiovascular risk parameters, and repair-type.

Results

Of 1655 patients, 1455 had sufficient quality imaging for FAVS (145 women, 1310 men). kNN clustering identified two morphological subtypes (n=878 and n=577), with sex imbalance (13.8% vs. 4.1% women, $p<0.001$). The clusters differed in wall thrombus burden in visceral vessels, infrarenal aorta, aneurysmal neck, and CIAs ($p<0.001$). On adjusted multivariate regression, there was no significant differences in thromboembolic events between clusters, although event rate was low (n=31, 2.1%) (OR 1.56, 95% CI 0.71–3.43, $p = 0.23$).

Conclusion

Unsupervised machine learning can identify distinct aneurysm morphological phenotypes with significant thrombus burden difference, which exhibit sex imbalance. While thromboembolic

events were infrequent and did not differ significantly between clusters, these anatomical phenotypes may provide a framework for future studies investigating embolic risk and sex-specific disease mechanisms.

Introduction

Abdominal aortic aneurysms (AAA) encompass a morphologically heterogenous group of aneurysmal diseases, characterised by various levels of vascular remodelling both within the aneurysm and adjacent visceral, and access vasculature (1). Current decision-making around AAA repair is multifactorial, incorporating patient fitness, comorbidities, and patient preferences, alongside anatomical considerations derived from preoperative imaging. For endovascular repair (EVAR), adherence to device-specific instructions for use (IFU) dependent on aneurysm morphology remains a key for eligibility (2). These traditional anatomical metrics such as vessel diameters still dominate risk stratification and procedural planning. However, these conventional measurements may not fully capture the complexity of aneurysm morphology or accurately predict the risk of adverse outcomes (3). Thrombo- and microembolic events causing cerebral, renal, bowel or limb ischaemia are often catastrophic sequalae of AAA repair, but are difficult to predict (4). It has been suggested that higher intraluminal thrombus burden, together with narrower more tortuous arteries of organ supply, increase vulnerability to thromboembolic and microembolic complications (5). However, there remain a paucity of evidence regarding risk factors for these events, and potential strategies for their prevention. Furthermore, accurate quantification of thrombus burden and other three-dimensional morphological parameters using manual techniques is time-consuming and labour-intensive, limiting their routine use in clinical decision-making (6,7).

Our reliance on simple measurements are partly due to limitations of current technique used in pre-operative planning, which is most commonly based on Computed Tomography Angiography (CTA) scanning, enabling assessment of vascular morphology. Optimal planning for AAA repair requires thin-slice, single arterial-phase CTA (≤1 mm), allowing orthogonal centreline-based diameter measurements (9). These conventional measurements remain the clinical standard for both endovascular and open repair. However, volumetric assessment, though not yet part of routine preoperative planning, is increasingly applied in post-EVAR surveillance, where sac volume changes can inform follow-up strategies. Fully automatic volume segmentation (FAVS) has been shown to be accurate, reproducible, and fast for assessment of AAA diameters and volume (7). What is more, FAVS results in rich radiomic datasets, which yield itself to analysis using machine learning methods, to elucidate complex interaction between geometric and volumetric variables. Comprehensive assessment of FAVS could enable detailed assessment of vascular anatomy, including additional features such as thrombus burden. These, in line, could be used to identify morphological subtypes amongst aneurysms, which when compared, could help in identification of additional morphological features associated with adverse outcomes. It is possible therefore that use of these more advanced morphological assessments may better predict risk of adverse AAA-related events, such as thrombo- and micro-embolism, than is currently achieved using conventional metrics.

The primary aim of this study was to use FAVS of CT imaging to investigate the existence of morphological subtypes amongst AAA, comparing them in terms of anatomical differences and differences in patient factors. The secondary aim was to compare the resulting morphological subtypes with regards to clinical outcomes.

Methods

Study design and setting

This was an observational retrospective cohort study conducted in three tertiary vascular centres based in the UK. All adult patients over 50 years old, receiving primary open or endovascular aortic repair (EVAR) for infra-renal AAA or juxta-renal AAA at a participating centre from 1/1/2013 to 01/07/2023 were included. Pre-operative CT imaging was extracted from participating centres. Patient demographic information, co-morbid status, indication for surgery, and outcomes were obtained locally from contemporaneously collected UK National Vascular Registry (NVR) records. Pre-existing variables are defined within the UK NVR data dictionary (10) and the OPCS Classification of Interventions and Procedures (11).

Exclusion criteria were: 1) insufficient CT imaging quality to enable automated segmentation (>1mm slices), or lack of CT imaging within 1 year of operation; 2) ruptured aneurysm, aorto-iliac occlusive disease, penetrating aortic ulcer, dissection or supra-renal AAA 3) secondary AAA repair; 4) patients with insufficient clinical data to enable risk stratification (e.g., lack of data regarding co-morbid status). Aortic size index (ASI) was defined as AAA diameter/body surface area (cm/m^2). Assessment of validity and correction and/or imputation of missing clinical data fields were performed locally by a member of the direct care team during clinical data extraction and pseudonymisation.

Fully automatic segmentation software was provided by PRAEVAorta, Nurea® which has received CE marking (Class IIb) (12). Use of PRAEVAorta for fully automatic volume segmentation has been shown to be fast and reproducible for evaluation of the infra-renal aorta both pre- and post-operatively (6,7,13). It has been validated in external cohort, and has shown excellent concordance with manual measurements (Dice similarity coefficient >0.9), and fast segmentation time (ranging from 27s to 4 min per patient) (6,7,13). Quality assurance for

automatic imaging segmentation was conducted in three stages. First, each scan was reviewed by a vascular surgeons not involved in the software development to confirm aneurysm presence and pre-operative status. Second, the resulting three-dimensional reconstructions were visually inspected to verify correct identification of the aorta and visceral branches. Finally, missing measurement fields and outlier values were assessed, and cases with segmentation failure (>10% missing data fields) or inaccurate vessel identification were excluded. Review of the initial clustering outputs was performed independently by vascular surgeons with expertise in complex aortic repair, blinded to all clinical outcomes.

Outcome measures

Primary outcome measures were vascular morphology: neck morphology (e.g., diameter, length, supra-renal angle, infrarenal angle), visceral and access vessel diameters, tortuosity index, calcification volume, wall thrombus index, thrombus volume and maximum common iliac artery stenosis. Wall thrombus index was defined as a proportion of thrombus volume compared with vessel volume at the level measured.

Secondary outcome measures were major post-operative ischaemic complications, defined as a composite endpoint including bowel ischaemia, limb ischaemia, and cerebral ischaemia events recorded during the index admission. These data were obtained from contemporaneous entries in the UK National Vascular Registry (NVR) and cross-checked by the local vascular clinical teams.

Data analysis

All analyses, including machine learning modelling were conducted using R statistical software (version 4.2.3) (14). A list of packages and example code utilised can be found in Supplementary Table 1. Missing data patterns were explored with assessment of the associations between

missing variables, patient sex and repair modality, and Upset plots illustrating intersections of missingness were created (15,16). Clinical variables with insufficient data quality (defined as >25% missing data), were excluded from further analyses. Due to observed difference in the degree of missingness between the sexes, imputation missing data was performed using a K-nearest neighbours (KNN) approach, with comparison of original and imputed data (17,18). To maintain methodological consistency and preserve inter-variable correlations, a single KNN imputation strategy was applied across all retained variables.

Following imputation, highly correlated variables (>0.9) were removed, and principal component analysis (PCA) was performed to achieve further dimensionality reduction (19). Contribution of each principal component was assessed quantitatively. Initial number of principal components was defined as number of variables divided by 2 (n/2), following which it was optimised through sequential trials, to achieve the highest silhouette score. Following PCA, machine learning approaches were used for clustering. Clinical covariates such as age, sex, and comorbidity status were intentionally excluded from the clustering input to allow the identification of purely anatomical phenotypes based solely on imaging-derived variables, thereby avoiding bias from predefined clinical features. Supervised machine learning approaches were discounted, due to low thromboembolic event rate, and risk of overfitting – instead unsupervised methods were favoured. These unsupervised ML methods included KNN, density-based spatial clustering of applications with noise (DBSCAN), gaussian mixture model (GMM) (20–22). Cluster quality was evaluated using silhouette score, with approach yielding highest silhouette score whilst utilising fewest possible clusters used for further analysis. Cluster separation was also inspected visually using UMAP plots in 2D scape, and through repeated the analysis using agglomerative hierarchical clustering with Ward linkage, assessing concordance with the k-means solution via adjusted Rand index. Following unsupervised clustering, the anatomical profiles of each cluster, and variables with highest weights on PCA were independently reviewed by two vascular

surgeons involved in the study. This review focused on the clinical recognisability of the patterns, particularly in relation to access vessel anatomy, aneurysm extent, and planning considerations for endovascular repair. This was done on a cluster basis, and not scan-by-scan basis.

Following clustering, standard parametric and non- parametric testing was then used to assess for inter-cluster differences in the pre-specified variables of interest, with a p-value of <0.05 considered significant. No-adjustment were made for multiple significance testing (e.g. Bonferroni or false discovery rate), however, grouping of 'familiar' variables (e.g., visceral vessel diameters, calcification volumes) was used to guide the level of confidence, with greater weight given to consistent findings across a 'familiar' variable group (23). This was to allow for detection of signals in this exploratory analysis, and follows previously outlined methodology (23). Post-hoc linear regression model was used to determine the effect of demographic variables with significant inter-cluster differences on cluster membership, using McFadden's $R^{2.}$

For secondary outcomes analysis first, cluster-stratified univariate analyses to examine the relation between each variable and the outcome of interest (thromboembolic event) were conducted. A threshold of $p<0.1$ or a pre-determined high likelihood of clinical or mechanistic significance were used to govern subsequent selection for multivariate analyses. Assessment of multicollinearity, using variance inflation factors (VIFs) were used to determine final variable selection, with a value >2 deemed significant (24).

The effect of cluster as the exposure was examined on the log odds of a major thromboembolic event and was defined as the ATT (average treatment effect on the treated), namely the causal effect of cluster on the outcome, and the within approach was utilised, meaning that matching and estimates of casual effects and standard errors were performed within each imputed dataset followed by pooling of the results.

Regulatory aspects and ethical approval

The project was approved by the Health Research Authority (HRA) and Health and Care Research Wales (HCRW) (IRAS: 292985, REC: 21/HRA/0498), and sponsored by Imperial College London. Data processing agreements and research services agreement were agreed by Nurea (company number RCS Bordeaux 841437411 00017, France) and Imperial College of Science, Technology and Medicine, who acted as sponsor for the study. DICOM data was pseudonymised by local care teams through removal of patient identifiable/personal meta-data, and replacement with a study identification number. All data for the project was stored securely on a password protected, GDPR compliant, secure cloud server, owned by Imperial College London, or on encrypted hard drives, stored in a locked location at Imperial College London. Pseudonymised DICOM data was securely transferred to Nurea's server for FAVS, following which, an output report was created and DICOM data was deleted. Nurea were not party to any identifiable, sensitive, or personal data. This study was conducted according to the STROBE and RECORD guidelines for observational studies (25,26) (Supplementary Table 2).

Results

Demographics and cohort characteristics

A total of 1655 patients at the 3 centres met all inclusion criteria, and 1455 had CTA imaging of sufficient quality for analysis. Of the 200 patients excluded, 161 had scan sequence insufficient for segmentation (e.g. non-contrast or >1mm slice thickness protocol), whilst 39 scans failed segmentation due to software limitation. Of these at total of 452 patients (40 women, 412 men) received an open repair and 1003 patients (105 women, 892 men) received an EVAR (Figure 1).

Clustering of morphological subtypes and cluster characteristics

Ten variables were removed from the analysis, due to high % of data missingness; all of them were functionally represented elsewhere in the dataset, as the software generates largely

duplicate ways of measuring related concepts (e.g. mean and median stenosis). Following PCA, two principal components yielded most accurate cluster separation across all methods of clustering, out of which KNN clustering with 2 clusters has achieved highest silhouette score, and most pronounced separation of visual inspection of the UMAP plots in 2D space. (0.4, Supplementary Figure 1). The algorithm generated 2 clusters; cluster 1 (n=878) and cluster 2 (n=557). Despite a moderate average silhouette score (0.4), cluster separation was visually evident in PCA space (Figure 2), and robustness was supported by alternative clustering approaches, with cluster membership remaining moderately stable across methods (adjusted Rand Index = 0.498).

Cluster 1 had significantly more women (13.8% vs 4.2%, p <0.001), lower median age (74 vs 76, p = 0.002), and higher proportion of patients with COPD (28.2% vs 20.1%, p= 0.001). There were no significant differences between clusters in the proportion of patients receiving antiplatelet therapy, anticoagulation, or statins at baseline. Full baseline characteristics of the clusters are presented in *Table 3.* In post-hoc logistic regression, both sex and age were independently associated with morphological phenotype assignment. Female sex was strongly associated with the cluster 1 membership (OR 3.83, 95% CI 2.48–6.15, p < 0.001), while increasing age was associated with a lower likelihood of such membership (OR 0.98 per year, 95% CI 0.96–0.99, p = 0.0017). Despite these significant associations, the model explained only ~2.6% of the variance in cluster assignment (McFadden's = 0.026), indicating that age and sex difference alone do not account for the observed clustering. Full logistic regression model can be found in Supplementary Table 3.

Cluster analysis is shown in Figure 2. Upon analysis of PCA and relative weights of variables in each PC, the top 10 variable contributors in PC1 were related to access vessel diameter (Right

and Left EIA and CIA lumen diameter), whilst in PC2 these were related to aortic neck or juxta renal diameter. Top PCA variable contribution data is available in Table 4.

Assessment of inter-cluster difference in vascular morphology

Clusters differed significantly in vascular morphology (Table 1). Patients in cluster 1 had narrower ($p<0.001$), and shorter aneurysmal necks ($p=0.005$), narrower visceral and access vessels ($p<0.001$), more stenosed CIAs ($p<0.001$). There were no clear patterns in vessel tortuosity index. Patients in cluster 2 had significantly more calcification in both their IIAs, right CIA, and aneurysmal neck ($p<0.05$).When wall thrombus index was compared, cluster 1 had significantly higher wall thrombus index in visceral, infrarenal and aneurysmal neck, as well as both CIA vessels ($p<0.01$) (Table 2). This is despite there being significantly higher thrombus volume in all those vessels in cluster 2 ($p<0.001$). Moreover, there was significantly more thrombus in right IIA amongst cluster 2 patients ($p<0.01$).

Assessment of inter-cluster differences in thromboembolic outcomes

Cluster 1 were observed to have a greater rate of post-operative thromboembolic events (e.g., limb ischaemia, bowel ischaemia, stroke) 2.6% vs 1.7%, $p = 0.35$ but event rates were low, and the observed differences were not significant. On univariate analyses, in addition to patient cluster, following variables were found to have an association with post-operative thromboembolic events: ASI, comorbidities (e.g., COPD, CKD,) smoking status, medications (e.g., antiplatelet), symptomatic AAA, treatment centre, treatment modality (open or EVAR), tortuosity of the thoracic aorta and neck, calcification of the neck, SMA, CIA and IIA, AWT index for the neck, infrarenal aorta, SMA and CIA and CIA stenosis. Two additional variables (abnormal ECG and statin prescription) were also included due to pre-specified clinical relevance. Subsequent analysis of the effect of cluster on post- operative thromboembolic events, adjusted for co-morbidity, vascular morphology and thrombus burden, suggested no

statistically significant difference in thromboembolic event rates between clusters (OR 1.56 95%CIs 0.71-3.43, p=0.23).

Discussion

Unsupervised machine learning applied to full automated volume segmentation of AAA imaging generated two distinct morphological subtypes, with mainly differed by their thrombus burden in aneurysmal neck, body, access and visceral vessels. These clusters were sex-imbalanced, with high thrombus wall index cluster having higher proportion of women. The clusters did not differ in thromboembolic event rate; although these events were few. The emergence of such clusters purely from anatomical features underscores the presence of intrinsic structural heterogeneity within AAA disease that is not captured by conventional diameter-based assessments.

These results highlight that AAA is not a monolithic disease but rather a morphologically and biologically heterogeneous condition. The identified clusters signify that subsets of AAA patients might have different aneurysm structures – for instance, a thrombus-rich, smaller-diameter phenotype versus a large-calibre, thrombus-poor phenotype. This concept is reinforced by emerging genetic evidence. Recent large-scale genomic have identified over 100 genetic risk loci for AAA, implicating diverse pathways in its pathogenesis (27). The associated genes point to a complex interplay of processes, including lipid metabolism, extracellular matrix remodelling, vascular development, inflammation, and TGF-β signalling, each of which might contribute differently to aneurysm formation in different individuals (27). Such findings underscore that there may be distinct morphological phenotypes of AAA driven by different predominant mechanisms. Further studies incorporating both molecular, and imaging techniques are required to examine these potential endotypes; for example, a subtype with high thrombus index that might be driven by a pro-thrombotic or inflammatory environment leading to rapid thrombus

deposition, versus another endotype that might be driven more by connective tissue degradation and vessel expansion.

Sex differences likely intersect with this heterogeneity. Beyond anatomic measurements, female AAAs have been previously suggested to behave differently at the tissue level: women's aneurysms tend to grow faster and rupture at smaller diameters than men's, suggesting potential intrinsic differences in wall biomechanics or remodelling capacity (28). Some studies have noted that, even at equal diameter, women's aneurysm walls may have lower tensile strength or different collagen composition, which could contribute to earlier rupture (29). Additionally, hormonal and immunologic factors (such as the loss of oestrogen's protective effect on vascular inflammation in post-menopausal women) likely play a role in the sex-based divergence in AAA biology (30). Women are also more likely to suffer thromboembolic events following AAA repair (e.g., bowel ischaemia, lower limb ischaemia) (31). Taken together, these observations support a view of AAA as a spectrum of disease influenced by genetic background, sex, and other patient-specific factors. Furthermore, aneurysm morphology may evolve with age, and future longitudinal work is required to understand whether these phenotypes shift over time or represent stable endotypes. Importantly, because our clustering was based exclusively on anatomical variables, age and sex were not inputs to the model, and their observed distribution across clusters should be interpreted as an emergent property rather than a driver of the clustering process.

This study demonstrates the utility of FAVS combined with unsupervised learning to phenotype AAAs. Advanced imaging software now allows rapid, reproducible quantification of aneurysm morphology beyond the aneurysm diameter (6). In our dataset, FAVS provided volumetric measures of thrombus, calcification, tortuosity, conventional metrics of diameters, neck angulation, and other features that would be tedious or prone to observer error if measured

manually. By leveraging these rich data with a clustering algorithm, we uncovered potentially novel anatomical subtypes that traditional measurements might overlook. What is more, although the clustering was data-driven, clinical review by vascular surgeons confirmed that the anatomical patterns reflected recognisable phenotypes that could carry practical implications for procedural planning and EVAR complexity. This data-driven approach could in the future augment clinical assessment and move us toward a more personalised or precision-medicine strategy in AAA management. Although the silhouette score of 0.4 suggested moderate cluster separation, the decision to adopt a two-cluster solution was also guided by clinical interpretability. The clustering separated patients primarily along two anatomical axes, iliac access vessel morphology, and neck morphology, which align with known technical considerations in EVAR planning. Further subdivision beyond two clusters did not yield clinically distinct or more stable phenotypes. Current clustering requires further validation, before clinical translation, but even in its current form, provides an insight into how such technology can be leveraged for patient benefit. For instance, identifying that a patient's aneurysm falls into a "high-thrombus, small-vessel" subtype (akin to Cluster 1) could influence preoperative planning. Endovascular repair in such a patient may warrant use of low-profile devices or adjunctive access techniques (e.g. iliac conduits or angioplasty) given the narrow iliac arteries (32). The increased thrombus burden might also prompt careful intraoperative imaging and handling to mitigate distal embolisation, or even consideration of alternative strategies if thrombus appears mobile. On the other hand, cluster 2 aneurysm with relatively less thrombus might prioritise concerns about maximal wall stress and rupture risk over embolic risk. In this way, anatomical clustering could in the future inform a tailored approach – selecting the right tools, anticipating complications, and counselling patients based on the particular subtype of AAA they harbour. Such stratification could enable going beyond the one-size-fits-all criterion of diameter >5.5 cm for repair, aligning with contemporary calls for toward individualised vascular care (33). Post-hoc modelling confirmed that sex and age are associated with cluster membership, supporting the

notion that biological differences, particularly sex-linked vascular characteristics, influence aneurysm morphology. However, the modest explanatory power (2.6%) of these variables suggests that anatomical heterogeneity extends beyond demographic factors alone. These findings underscore the need for future work integrating demographic, molecular, and anatomical data to refine phenotype definitions and better understand their underlying mechanisms. Interestingly, thrombus metrics emerged as key drivers differences between cluster, which suggests that intraluminal thrombus is an important morphological differentiator among AAAs. As automated segmentation and machine learning tools become more integrated into vascular imaging workflows, they could continually refine such classifications, eventually enabling real-time identification of an aneurysm's subtype during routine CT evaluation. While thromboembolic and microembolic complications remain clinically important, this study was not powered to evaluate outcome differences, and no statistically significant differences were observed between phenotypes. These findings should therefore be interpreted as exploratory and hypothesis-generating. Larger, prospectively designed studies will be required to investigate whether morphological endotypes influence embolic risk or other clinical outcomes (34).

Although exploratory, the clustering framework presented here may offer a foundation for future stratification tools in AAA management. Translation into clinical care would require external validation, integration with risk prediction models, and evaluation of procedural and long-term outcomes by cluster type. The morphological phenotypes identified in this study could be incorporated into preoperative decision-making, through variety of technical considerations such as early the use of low-profile endografts, planned iliac conduits, alternative access routes to avoid intraoperative vessel injury, or staged procedures. Integration of cluster classification into CTA reporting or pre-operative planning could provide a rapid anatomical "risk map" to support multidisciplinary discussions, aligning device selection and perioperative strategy with the specific anatomical challenges posed by each patient. What is more, such risk stratification

could prompt referral to specialist tertiary or quaternary centres for 'very high risk' cases, as well as altered peri-operative anticoagulation strategies, or statin dose adjustment. Further, should validation in a larger cohort but successful, supervised ML approaches can be considered to produce a numerical risk score for thromboembolic events, which could be factored into discussions with patients, and management strategies. We plan on developing a continuous morphology score and clinically meaningful thresholds will be and prospectively test it for associations with predefined outcomes and incremental predictive value beyond current criteria. If validated, these phenotypes could inform procedural planning and patient selection in future multicentre studies and phenotype-guided clinical trials. While this remains an early-stage application, it illustrates a pathway by which unsupervised phenotyping could evolve from an exploratory research tool to a practical adjunct in individualised AAA management.

This study has several limitations. First, our analysis was retrospective and observational, thus it is possible that unmeasured confounding factors influenced both aneurysm morphology and outcomes. It was also limited by the datapoints included in NVR, and relative lack of granularity in type of EVAR device use, technical steps and adjuncts used during procedures, and complication data. Second, the clustering methodology itself has constraints. We selected a two-cluster solution for its clinical interpretability and consistency with known binary contrasts (e.g., high vs. low thrombus burden), but the optimal number of clusters in AAA morphology is not definitively known. The moderate silhouette score of our clustering (~0.4) indicates only modest separation between the two groups, implying that AAA anatomical features may exist on a continuum rather than in clearly discrete categories. This is further supported by the moderate adjusted Rand Index, suggesting cluster stability, but not perfect alignment (0.498). Some aneurysms in our cohort had intermediate features that could plausibly fit in either cluster, reflecting the inherent variability of the disease, that could represent a spectrum, rather than two (or more) distinct risk groups. However, a three-cluster classification shown less discrimination in

exploratory analyses, and the clusters demonstrated distinct and clinically plausible profiles, particularly in iliac and neck morphologies. Similar results using hierarchical clustering support the internal consistency of the two-cluster solution within this cohort, although external validation is required for confirming generesability and cluster stability. Future studies might also include additional features (such as biomechanical stress metrics or genetic markers) to see if more distinct subtypes can be identified. An important additional limitation of our approach is that clustering was based entirely on anatomical variables, without incorporating sex, age, or comorbidities. While this allowed us to define purely anatomical phenotypes, it also introduces the potential for residual confounding. As such, the relationship between cluster membership and clinical outcomes should be interpreted as exploratory, although we have attempted to mitigate this through regression. Future studies with larger cohorts should consider multivariable adjustment to delineate the independent contribution of anatomical phenotype. Fourth, although the overall cohort was large, the number of observed thromboembolic events was relatively low (n=31), limiting statistical power to detect meaningful differences between clusters. A post hoc power calculation based on the observed event rates (2.6% in cluster 1 vs. 1.7% in cluster 2) and sample sizes (n_1 = 878, n_2 = 577) indicated a statistical power of 21.4% at a two-sided alpha of 0.05. This low power underscores that these findings should be viewed as exploratory and hypothesis-generating rather than confirmatory. What is more, the composite definition of thromboembolic events used in this study encompassed outcomes with diverse mechanisms, some of which may not be directly related to aneurysm morphology (e.g., clamp-related limb ischaemia or procedure-associated cerebral events). While this approach aimed to capture the full spectrum of clinically relevant ischaemic complications, it introduces heterogeneity and potential confounding, and any associations observed should therefore be interpreted cautiously. This has also limited the ability to analyse the data using supervised machine learning methods, without risking model overfitting. Future studies with greater event rates or larger cohorts will be necessary to validate this potential association. Due to exploratory nature of the study, and to

allow for broader hypothesis generation, we have not applied statistical multiple testing adjustments. As a result, the reported findings may have an increased false discovery rate. It's worth acknowledging that a proportion of scans could not be segmented accurately, despite a correct scanning protocol (n=39/1655, 2.3%). Majority of exclusions (n=161) this was due to imaging quality, especially in light of inclusion of cases which have underwent open surgical repair and have not had thin slice CTA required for segmentation, yet segmentation failure it reflects current limitations of FAVS algorithms. This challenge is increasingly recognised in the field of FAVS, as shown in the recent study by van Tongeren et al., who demonstrated the need for continued refinement of both imaging protocols and software performance (37). Finally, our analysis focused on anatomical and volumetric data from CT imaging; we did not incorporate further radiomic features into the analysis, which could have proved informative when looking into thrombus morphology.

Conclusion

Unsupervised machine learning applied to fully automated imaging data can identify distinct abdominal aortic aneurysm morphological phenotypes characterised by differences in thrombus burden, vessel calibre, and sex distribution. These phenotypes emerge independently of clinical variables and highlight the underlying anatomical heterogeneity of AAA disease. Although no statistically significant differences in thromboembolic outcomes were observed, this approach provides a framework for future studies aimed at integrating anatomical phenotyping with clinical, molecular, and biomechanical data. Further work is needed to determine whether such phenotypes have predictive or therapeutic relevance in AAA management.

Disclosures:

Conflicts of Interest: none declared

Acknowledgements: ALP was supported by NIHR Doctoral Fellowship to conduct this research.

Data availability statement: The summary data underlying this article will be shared on reasonable request to the corresponding author.

References

1. Bhagavan D, Di Achille P, Humphrey JD. Strongly Coupled Morphological Features of Aortic Aneurysms Drive Intraluminal Thrombus. Sci Rep. 2018 Sept 5;8(1):13273.

2. Grassl K, Gasser TC, Enzmann FK, Gratl A, Klocker J, Wippel D, et al. Early Prediction of Abdominal Aortic Aneurysm Rupture Risk Using Numerical Biomechanical Analysis. Diagnostics. 2024 Dec 26;15(1):25.

3. Diender E, Vermeulen JJM, Pisters R, van Schaik PM, Reijnen MMPJ, Holewijn S. Major adverse cardiac events after elective infrarenal endovascular aortic aneurysm repair. J Vasc Surg. 2022 Dec 1;76(6):1527-1536.e3.

4. Simmering JA, de Vries M, Haalboom M, Reijnen MMPJ, Slump CH, Geelkerken RH. Geometrical Changes of the Aorta as Predictors for Thromboembolic Events After EVAR With the Anaconda Stent-Graft. J Endovasc Ther. 2023 Dec 1;30(6):904–19.

5. Pouncey AL, Khan A, Alharahsheh B, Bicknell C, Powell JT. Editor's Choice - Hypothesis for the Increased Rate of Thromboembolic and Microembolic Complications Following Abdominal Aortic Aneurysm Repair in Women. Eur J Vasc Endovasc Surg Off J Eur Soc Vasc Surg. 2022 Feb;63(2):348–9.

6. Caradu C, Spampinato B, Vrancianu AM, Bérard X, Ducasse E. Fully automatic volume segmentation of infrarenal abdominal aortic aneurysm computed tomography images with deep learning approaches versus physician controlled manual segmentation. J Vasc Surg. 2021 July;74(1):246-256.e6.

7. Caradu C, Pouncey AL, Lakhlifi E, Brunet C, Bérard X, Ducasse E. Fully automatic volume segmentation using deep learning approaches to assess aneurysmal sac evolution after infrarenal endovascular aortic repair. J Vasc Surg. 2022 Sept;76(3):620-630.e3.

8. Picel AC, Kansal N. Essentials of endovascular abdominal aortic aneurysm repair imaging: preprocedural assessment. AJR Am J Roentgenol. 2014 Oct;203(4):W347-357.

9. Ristow I, Riedel C, Lenz A, Well L, Adam G, Panuccio G, et al. Current Imaging Strategies in Patients with Abdominal Aortic Aneurysms. ROFO Fortschr Geb Rontgenstr Nuklearmed. 2024 Jan;196(1):52–61.

10. VSQIP - Vascular Services Quality Improvement Programme [Internet]. 2025 [cited 2025 Mar 14]. NVR Data Dictionary. Available from: https://www.vsqip.org.uk/resource/nvr-data-dictionary/

11. OPCS-4.10 [Internet]. [cited 2025 Mar 14]. Available from: https://classbrowser.nhs.uk/#/book/OPCS-4.10

12. AI solution for vascular diseases | Nurea [Internet]. [cited 2025 Mar 14]. Available from: https://nurea-soft.com/

13. Pouncey AL, Charles E, Bicknell C, Bérard X, Ducasse E, Caradu C. Fully Automatic Volume Segmentation Using Deep Learning Approaches to Assess the Thoracic Aorta, Visceral Abdominal Aorta, and Visceral Vasculature. Eur J Vasc Endovasc Surg. 2025 Aug;

14. R: A Language and Environment for Statistical Computing. R Foundation for Statistical Computing, Vienna. [Internet]. R Core Team; 2022. Available from: https://www.R-project.org

15. Lex A, Gehlenborg N, Strobelt H, Vuillemot R, Pfister H. UpSet: Visualization of Intersecting Sets. IEEE Trans Vis Comput Graph. 2014 Dec;20(12):1983–92.

16. Conway JR, Lex A, Gehlenborg N. UpSetR: an R package for the visualization of intersecting sets and their properties. Bioinformatics. 2017 Sept 15;33(18):2938–40.

17. Kuhn M, Johnson K. Applied Predictive Modeling [Internet]. New York, NY: Springer New York; 2013 [cited 2025 Mar 14]. Available from: http://link.springer.com/10.1007/978-1-4614-6849-3

18. Ho D, Imai K, King G, Stuart EA. MatchIt: Nonparametric Preprocessing for Parametric Causal Inference. J Stat Softw. 2011 June 14;42:1–28.

19. Jolliffe IT, Cadima J. Principal component analysis: a review and recent developments. Philos Transact A Math Phys Eng Sci. 2016 Apr 13;374(2065):20150202.

20. Ester M, Kriegel HP, Xu X. A Density-Based Algorithm for Discovering Clusters in Large Spatial Databases with Noise.

21. Yu G, Sapiro G, Mallat S. Solving Inverse Problems with Piecewise Linear Estimators: From Gaussian Mixture Models to Structured Sparsity [Internet]. arXiv; 2010 [cited 2025 Apr 20]. Available from: http://arxiv.org/abs/1006.3056

22. Cover T, Hart P. Nearest neighbor pattern classification. IEEE Trans Inf Theory. 1967 Jan;13(1):21–7.

23. Streiner DL. Best (but oft-forgotten) practices: the multiple problems of multiplicity-whether and how to correct for many statistical tests. Am J Clin Nutr. 2015 Oct;102(4):721–8.

24. Fox J, and Monette G. Generalized Collinearity Diagnostics. J Am Stat Assoc. 1992 Mar 1;87(417):178–83.

25. von Elm E, Altman DG, Egger M, Pocock SJ, Gøtzsche PC, Vandenbroucke JP, et al. Strengthening the Reporting of Observational Studies in Epidemiology (STROBE) statement: guidelines for reporting observational studies. BMJ. 2007 Oct 20;335(7624):806–8.

26. Benchimol EI, Smeeth L, Guttmann A, Harron K, Moher D, Petersen I, et al. The REporting of studies Conducted using Observational Routinely-collected health Data (RECORD) statement. PLoS Med. 2015 Oct;12(10):e1001885.

27. Roychowdhury T, Klarin D, Levin MG, Spin JM, Rhee YH, Deng A, et al. Genome-wide association meta-analysis identifies risk loci for abdominal aortic aneurysm and highlights PCSK9 as a therapeutic target. Nat Genet. 2023 Nov;55(11):1831–42.

28. DiLosa K, Brittenham G, Pozolo C, Hedayati N, Kwong M, Maximus S, et al. Evaluating growth patterns of abdominal aortic aneurysms among women. J Vasc Surg. 2024 July 1;80(1):107–13.

29. Larsson E, Labruto F, Gasser TC, Swedenborg J, Hultgren R. Analysis of aortic wall stress and rupture risk in patients with abdominal aortic aneurysm with a gender perspective. J Vasc Surg. 2011 Aug;54(2):295–9.

30. Wu XF, Zhang J, Paskauskas S, Xin SJ, Duan ZQ. The role of estrogen in the formation of experimental abdominal aortic aneurysm. Am J Surg. 2009 Jan;197(1):49–54.

31. Pouncey AL, David M, Morris RI, Ulug P, Martin G, Bicknell C, et al. Editor's Choice - Systematic Review and Meta-Analysis of Sex Specific Differences in Adverse Events After Open and Endovascular Intact Abdominal Aortic Aneurysm Repair: Consistently Worse Outcomes for Women. Eur J Vasc Endovasc Surg Off J Eur Soc Vasc Surg. 2021 Sept;62(3):367–78.

32. Sampaio SM, Panneton JM, Mozes GI, Andrews JC, Noel AA, Karla M, et al. Endovascular abdominal aortic aneurysm repair: does gender matter? Ann Vasc Surg. 2004 Nov;18(6):653–60.

33. Wanhainen A, Van Herzeele I, Bastos Goncalves F, Bellmunt Montoya S, Berard X, Boyle JR, et al. Editor's Choice -- European Society for Vascular Surgery (ESVS) 2024 Clinical Practice Guidelines on the Management of Abdominal Aorto-Iliac Artery Aneurysms. Eur J Vasc Endovasc Surg. 2024 Feb;67(2):192–331.

34. Hans SS, Jareunpoon O, Balasubramaniam M, Zelenock GB. Size and location of thrombus in intact and ruptured abdominal aortic aneurysms. J Vasc Surg. 2005 Apr;41(4):584–8.

35. van Voorst H, Bruggeman AAE, Yang W, Andriessen J, Welberg E, Dutra BG, et al. Thrombus radiomics in patients with anterior circulation acute ischemic stroke undergoing endovascular treatment. J Neurointerventional Surg. 2023 Sept;15(e1):e79–85.

36. Bhagavan D, Di Achille P, Humphrey JD. Strongly Coupled Morphological Features of Aortic Aneurysms Drive Intraluminal Thrombus. Sci Rep. 2018 Sept 5;8(1):13273.

37. Van Tongeren OLRM, Vanmaele A, Rastogi V, Hoeks SE, Verhagen HJM, De Bruin JL. Volume Measurements for Surveillance after Endovascular Aneurysm Repair using Artificial Intelligence. Eur J Vasc Endovasc Surg. 2025 Jan;69(1):61–70.

Table 1 – *Comparison of vascular morphology for cluster 1 and cluster 2. Abbreviations: CIA – common iliac artery, EIA – external iliac artery, IIA – internal iliac artery, AAA –abdominal aortic aneurysm, IQR – Interquartile Range.*

	Cluster 1	Cluster 2	**p-value**
n	878	577	
AAA Neck (median (IQR))			
Neck Diameter (mm)	23.64 [21.44, 26.31]	25.64 [23.44, 28.69]	<0.001
Maximum Neck Diameter (mm)	28.72 [26.05, 31.91]	31.11 [28.40, 34.93]	<0.001
Minimum Neck Diameter (mm)	21.94 [20.05, 24.25]	23.66 [21.81, 26.47]	<0.001
Neck Length (mm)	27.20 [17.39, 37.89]	29.76 [17.69, 41.64]	0.005
Neck Angle (degree)	33.12 [25.31, 41.80]	32.80 [24.68, 43.27]	0.768
Vessel Diameters (median (IQR))			
Coeliac Artery (mm)	6.85 [5.96, 7.81]	7.27 [6.44, 8.47]	<0.001
Superior Mesenteric Artery (mm)	6.50 [5.72, 7.31]	7.44 [6.56, 8.22]	<0.001
Left Renal Artery (mm)	4.73 [4.05, 5.53]	5.25 [4.57, 5.95]	<0.001
Right Renal Artery (mm)	4.46 [3.86, 5.15]	4.99 [4.27, 5.63]	<0.001
Left CIA (mm)	12.86 [11.55, 14.15]	17.36 [15.33, 19.91]	<0.001
Right CIA (mm)	13.40 [12.01, 14.84]	17.64 [15.56, 20.32]	<0.001
Left EIA (mm)	8.27 [7.42, 9.14]	10.14 [9.29, 10.98]	<0.001
Right EIA (mm)	8.20 [7.43, 9.10]	10.07 [9.23, 10.98]	<0.001
Left IIA (mm)	6.84 [5.79, 7.91]	9.15 [7.71, 10.53]	<0.001
Right IIA (mm)	6.93 [5.94, 7.99]	8.99 [7.80, 10.48]	<0.001
CIA Stenosis % (median (IQR))			
Right CIA	13.93 [10.21, 18.47]	12.49 [8.76, 17.31]	<0.001

Left CIA	11.74 [8.30, 16.94]	10.39 [7.64, 14.49]	<0.001
Tortuosity Index (median (IQR))			
Thoracic Aorta	1.20 [1.03, 1.29]	1.23 [1.05, 1.31]	<0.001
Neck	1.01 [1.00, 1.02]	1.01 [1.00, 1.02]	0.035
Coeliac Artery	1.05 [1.01, 1.10]	1.04 [1.02, 1.10]	0.664
Superior Mesenteric Artery	1.04 [1.02, 1.08]	1.04 [1.02, 1.07]	0.362
Left Renal Artery	1.08 [1.04, 1.17]	1.09 [1.04, 1.18]	0.614
Right Renal Artery	1.10 [1.05, 1.16]	1.11 [1.05, 1.18]	0.256
Infrarenal Aorta	1.08 [1.06, 1.12]	1.08 [1.05, 1.12]	0.944
Left CIA	1.08 [1.03, 1.15]	1.07 [1.03, 1.13]	0.026
Right CIA	1.06 [1.03, 1.12]	1.08 [1.03, 1.14]	0.021
Left EIA	1.13 [1.09, 1.20]	1.17 [1.12, 1.25]	<0.001
Right EIA	1.16 [1.10, 1.24]	1.23 [1.15, 1.33]	<0.001
Left IIA	1.12 [1.06, 1.22]	1.12 [1.06, 1.23]	0.544
Right IIA	1.09 [1.04, 1.17]	1.11 [1.05, 1.19]	0.006
Calcification, cm^3 (median (IQR))			
Neck	0.04 [0.00, 0.17]	0.05 [0.00, 0.20]	0.049
Left Renal Artery	0.00 [0.00, 0.00]	0.00 [0.00, 0.00]	0.929
Right Renal Artery	0.00 [0.00, 0.00]	0.00 [0.00, 0.00]	0.555
Left CIA	0.22 [0.06, 0.44]	0.26 [0.09, 0.47]	0.069
Right CIA	0.25 [0.09, 0.50]	0.30 [0.11, 0.57]	0.014
Left IIA	0.04 [0.00, 0.13]	0.06 [0.01, 0.17]	0.001
Right IIA	0.02 [0.00, 0.10]	0.04 [0.00, 0.13]	0.001

Table 2 – *Comparison of aortic wall thrombus index and thrombus volumes for cluster 1 and cluster 2. Abbreviations: CIA – common iliac artery, EIA – external iliac artery, IIA – internal iliac artery, aneurysm, IQR – Interquartile Range.*

	Matched cohorts (ASI)		
	Cluster 1	**Cluster 2**	**p-value**
n	878	577	
Wall Thrombus Index (median (IQR))			
Thoracic Aorta	4.33 [2.77, 7.13]	4.14 [2.60, 6.83]	0.064
Visceral Aorta	31.29 [22.01, 41.06]	24.82 [16.00, 34.51]	<0.001
Neck	16.57 [12.00, 22.62]	14.08 [10.94, 19.05]	<0.001
Coeliac Artery	4.97 [2.16, 8.86]	4.57 [1.92, 7.52]	0.022
Superior Mesenteric Artery	4.07 [1.72, 7.73]	4.41 [1.85, 7.64]	0.864
Left Renal Artery	6.43 [2.30, 12.32]	6.87 [2.34, 13.58]	0.599
Right Renal Artery	4.86 [1.70, 10.18]	4.55 [1.25, 9.44]	0.162
Infrarenal Aorta	51.36 [38.09, 62.75]	42.82 [27.28, 56.67]	<0.001
Left CIA	22.85 [16.70, 31.41]	20.53 [14.87, 28.43]	<0.001
Right CIA	25.08 [18.93, 33.32]	24.27 [16.49, 32.62]	0.027
Left EIA	7.10 [4.16, 12.27]	7.93 [4.41, 12.72]	0.184
Right EIA	7.67 [4.24, 13.19]	7.77 [4.45, 12.82]	0.969
Left IIA	14.97 [6.76, 24.33]	15.20 [8.41, 22.41]	0.455
Right IIA	11.57 [4.80, 20.71]	13.43 [7.17, 22.14]	0.002
Thrombus Volume cm^3 (median (IQR))			
Thoracic Aorta	4.50 [2.89, 6.61]	5.26 [3.44, 7.93]	<0.001
Neck	1.83 [1.04, 3.13]	1.96 [1.07, 3.20]	0.366
Infrarenal Aorta	96.99 [63.81, 143.66]	94.90 [49.43, 153.24]	0.347

Left CIA	1.32 [0.92, 2.05]	2.28 [1.50, 3.74]	<0.001
Right CIA	1.69 [1.17, 2.46]	2.85 [1.90, 4.23]	<0.001

Table 3 – *Baseline characteristics between clusters.*

	Cluster 1	*Cluster 2*	*p*
n	*878*	*577*	
Age (median [IQR])	*74.00 [69.00, 79.00]*	*76.00 [69.70, 80.60]*	*0.002*
Female, n(%)	*121 (13.8)*	*24 (4.2)*	*<0.001*
Diabetes, n(%)	*120 (13.7)*	*89 (15.4)*	*0.391*
HTN, n(%)	*635 (72.3)*	*390 (67.6)*	*0.061*
COPD, n(%)	*248 (28.2)*	*116 (20.1)*	*0.001*
IHD, n(%)	*293 (33.4)*	*175 (30.3)*	*0.247*
HF, n(%)	*44 (5.0)*	*37 (6.4)*	*0.306*
CKD, n(%)	*87 (9.9)*	*58 (10.1)*	*1*
Stroke, n(%)	*57 (6.5)*	*26 (4.5)*	*0.138*
Cancer, n(%)	*37 (4.2)*	*28 (4.9)*	*0.655*
PAD, n(%)	*16 (1.8)*	*5 (0.9)*	*0.204*
ASA (%)			*0.515*
1	*5 (0.6)*	*2 (0.3)*	
2	*160 (18.2)*	*118 (20.5)*	
3	*668 (76.2)*	*421 (73.1)*	
4	*43 (4.9)*	*35 (6.1)*	
5	*1 (0.1)*	*0 (0.0)*	
Hypalbuminaemia, n(%)	*122 (22.3)*	*102 (29.1)*	*0.028*
Anaemia, n(%)	*192 (25.8)*	*153 (30.8)*	*0.064*
Abnormal ECG, n(%)	*210 (24.2)*	*167 (29.3)*	*0.039*
Smoking Status, n(%)			*0.004*
Current Smoker	*207 (23.7)*	*99 (17.2)*	
Non-smoker	*550 (62.9)*	*375 (65.2)*	
Ex-smoker	*118 (13.5)*	*101 (17.6)*	
Statin, n(%)	*707 (80.5)*	*454 (78.7)*	*0.430*
Beta Blocker, n(%)	*259 (29.5)*	*172 (29.8)*	*0.946*
ACEi, n(%)	*276 (31.4)*	*175 (30.3)*	*0.698*
Anticoagulation, n(%)			*0.244*
0 agents	*148 (16.9)*	*108 (18.7)*	
1 agent	*723 (82.3)*	*460 (79.7)*	
2+ agents	*7 (0.8)*	*9 (1.6)*	
Antiplatelet, n(%)	*716 (81.5)*	*445 (77.1)*	*0.057*

ASI (median [IQR])	*3.14 [2.86, 3.57]*	*3.13 [2.76, 3.59]*	*0.274*
AAA Size (median [IQR])	*61.71 [58.59, 66.95]*	*63.67 [59.47, 71.90]*	*<0.001*
Symptomatic AAA, n(%)	*70 (8.0)*	*32 (5.5)*	*0.095*
Repair Type, n(%)			*0.370*
Open	*275 (31.3)*	*177 (30.7)*	
EVAR	*517 (58.9)*	*330 (57.2)*	
Complex EVAR	*86 (9.8)*	*70 (12.1)*	
MACE, n(%)	*42 (4.8)*	*18 (3.1)*	*0.154*
MACED, n(%)	*46 (5.2)*	*22 (3.8)*	*0.257*
Mortality, n(%)	*14 (1.6)*	*8 (1.4)*	*0.921*
Thromboembolic events, n(%)	*23 (2.6)*	*10 (1.7)*	*0.352*
MAE, n(%)	*68 (7.7)*	*39 (6.8)*	*0.547*
Centre , n(%)			*0.706*
Cambridge	*482 (54.9)*	*308 (53.4)*	
Imperial	*107 (12.2)*	*67 (11.6)*	
Leicester	*289 (32.9)*	*202 (35.0)*	

HTN – Hypertension. COPD – Chronic Obstructive Pulmonary Disease. IHD – Ischaemic Heart Disease. HF – Heart Failure. CKD – Chronic Kidney Disease. PAD – Peripheral Artery Disease. ASA – American Society of Anaethesiologists. ASI – Aortic Size Index. EVAR – Endovascular Aortic Repair. MACE – Major Adverse Cardiac Events. MACED. Major Adverse Cardiac Events and Death. MAE – Major Adverse Events.

Table 4 – *Top Contributors to principal component 1 & principal component 2*

	PC1	*PC2*
Top contributors to Principal Component 1		
Left CIA Mean Diameter	***0.75***	*-0.22*
Right EIA Mean Diameter	***0.74***	*-0.16*
Left CIA Minimum Diameter	***0.72***	*-0.24*
Left CIA Lumen Mean Diameter	***0.72***	*-0.21*
Left CIA Cross Sectional Mean Diameter	***0.71***	*-0.16*
Right CIA Lumen Mean Diameter	***0.71***	*-0.22*
Left CIA Max Diameter	***0.70***	*-0.14*
Left CIA Lumen Max Diameter	***0.70***	*-0.11*
Left CIA Lumen Minimum Diameter	***0.70***	*-0.22*
Right CIA Mean Diameter	***0.70***	*-0.24*
Top contributors to Principal Component 2		
Neck Maximum Diameter	*0.31*	***0.78***
Juxtarenal Aorta Max Diameter	*0.38*	***0.76***

Infrarenal Aorta Lumen Diameter	*0.35*	***0.73***
Neck Mean Diameter	*0.29*	***0.72***
Neck Minimum Diameter	*0.29*	***0.72***
Juxta renal Aorta Lumen Mena Diameter	*0.43*	***0.71***
Visceral Aorta Mean Diameter	*0.40*	***0.70***
Neck Lumen Mean Diameter	*0.37*	***0.69***
Infrarenal Aorta Mean Diameter	*0.29*	***0.67***
Neck Lumen Mean Diameter	*0.38*	***0.65***

1 *CIA – Common Iliac Artery. EIA – External Iliac Artery. PC – principal component.*

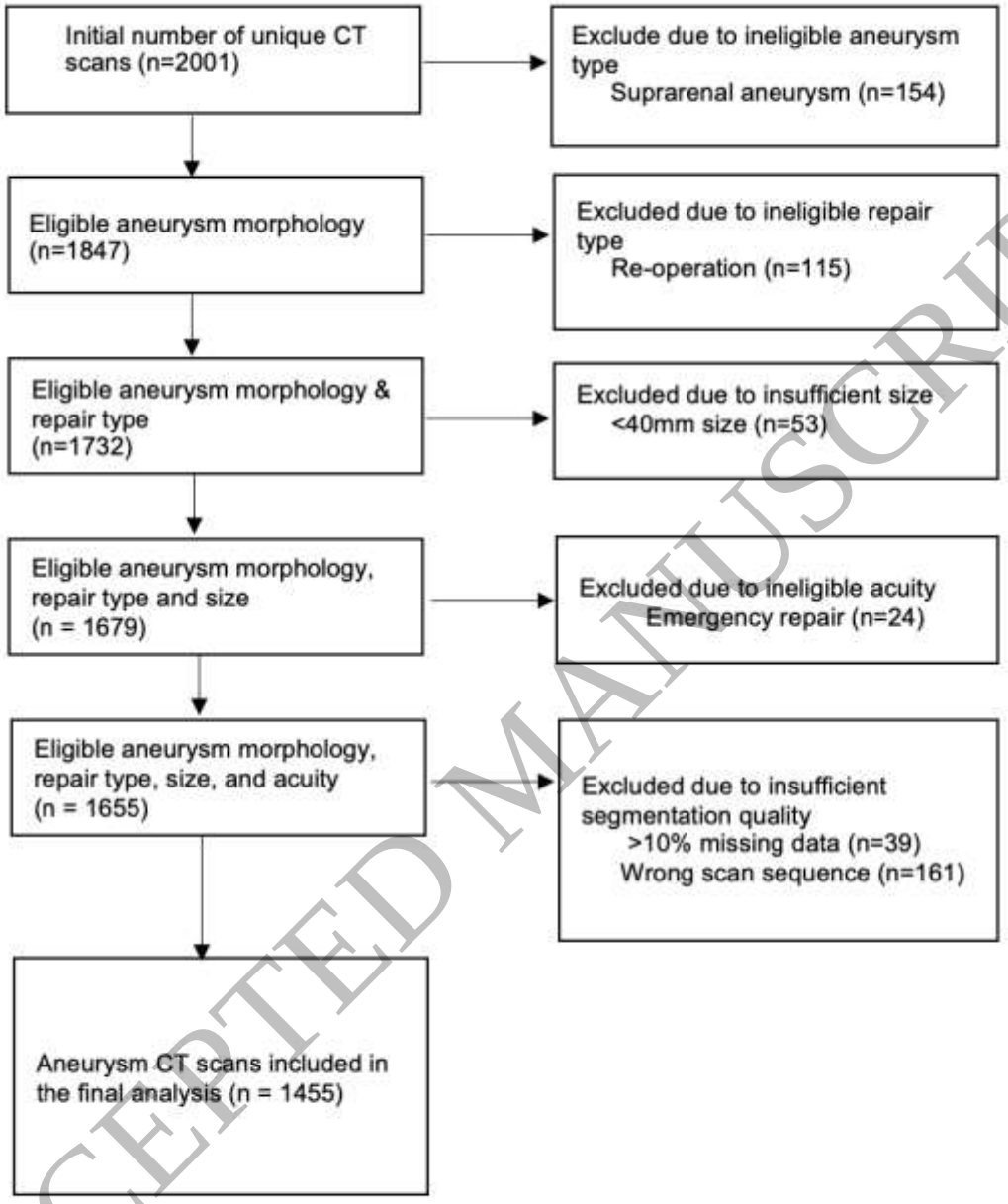

Figure 1 – Flow Diagram demonstrating patient selection. Abbreviations: AAA – abdominal aortic aneurysm, EVAR – endovascular aortic repair.

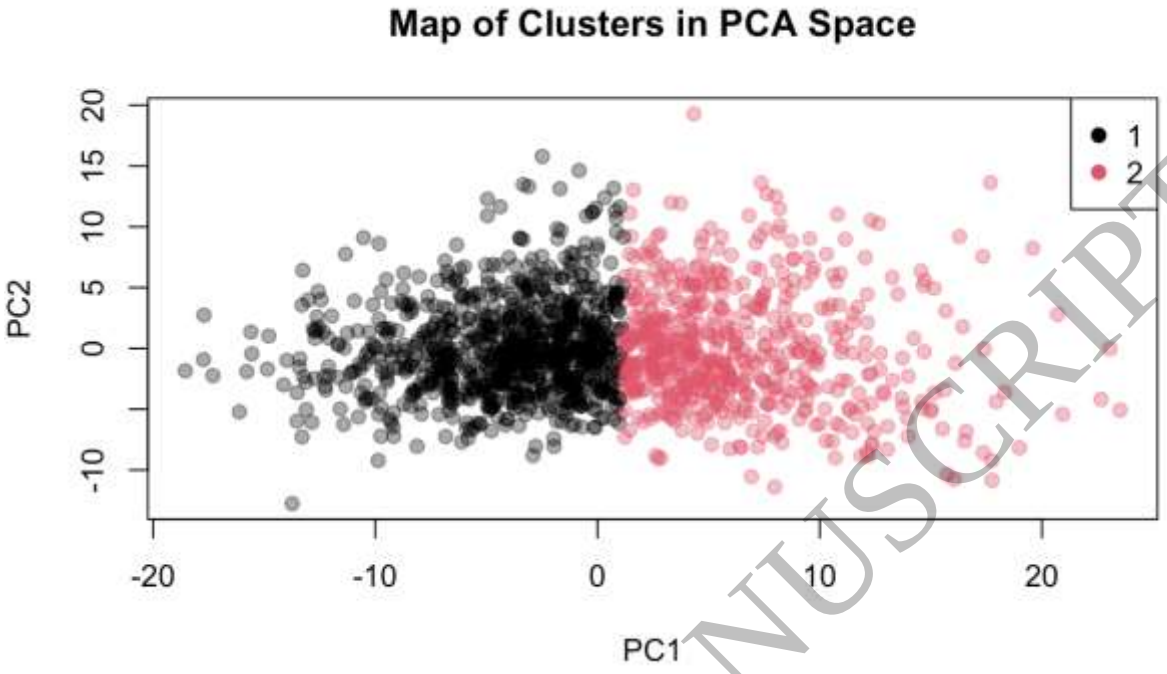

Figure 2 – UMAP Plot for Clusters. Cluster 1 in Black, Cluster 2 in Red. PC – Principal Component.

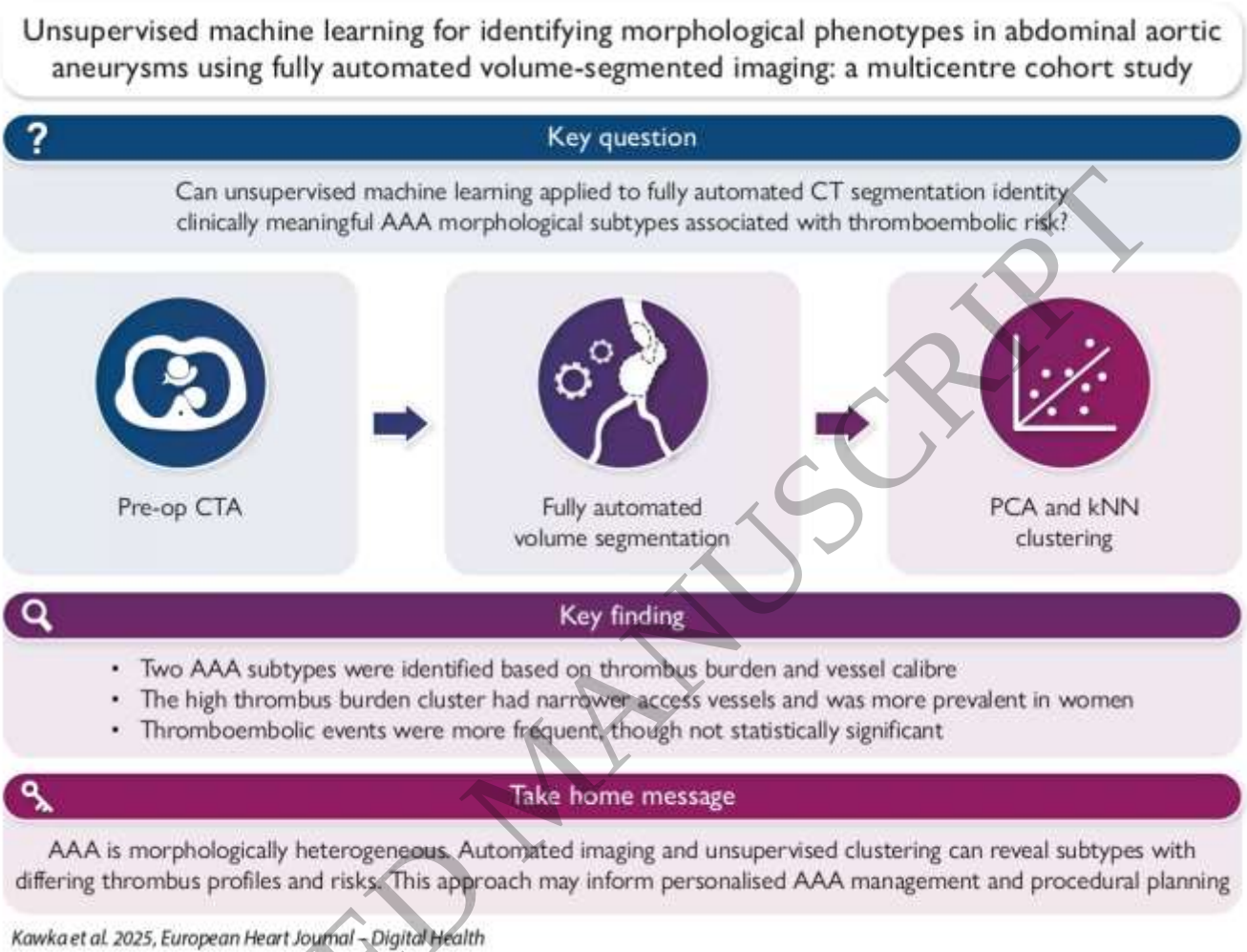

Graphical Abstract
180x135 mm (x DPI)

Mr Michal Kawka is an NIHR Academic Clinical Fellow in Vascular Surgery at City, St George's University of London. He was graduated from Imperial College London in 2023. His research interests lie in the use of data, and artificial intelligence for clinical outcomes research in aortic, and peripheral arterial diseases, and evaluation of novel surgical technologies.